Experimental Study on Scour at a Sharp-Nose Bridge Pier with Debris Blockage

Mohsen Ebrahimi, A.M.ASCE[1]; Prakash Kripakaran[2]; Dušan M. Prodanović[3]; Recep Kahraman[4]; Matthew Riella[5]; Gavin Tabor[6]; Scott Arthur[7]; and Slobodan Djordjević[8]

Abstract: Previous experimental research on the effects of debris on pier scour has focused primarily on circular and rectangular piers with debris present just under flow free surface. Debris-induced scour around sharp-nose piers, which are typical of masonry bridge piers, and the effect of debris elevation on pier scour have seldom been studied before. This paper aims to fill this knowledge gap. It presents results from flume experiments investigating scour around a sharp-nose pier under shallow flow conditions with angle of attack relative to the pier being zero. Uniform sand is used as bed material. Debris is modeled as stationary and extending only upstream of the pier. Three simplified debris geometries (cylinder, half-pyramid, and plate) are studied. Results show that scour depth decreases as debris gets closer to the bed with maximum scour depth occurring when debris is located just under the flow free surface. Interestingly, scour depths produced by debris in shallow flow are observed to be comparable to those produced by deep flow in the absence of debris. This finding highlights the importance of monitoring debris accumulation at bridges in nonflood conditions. Results also show that the volume of the scour hole around a pier increases quadratically with maximum scour depth. This information is useful for postflood scour remedial works. Lastly, the collected laboratory measurements are used to compare four popular equations for scour estimation on their ability to predict debris-induced scour. The Colorado State University (CSU) equation is found to offer the most accurate predictions. **DOI: 10.1061/(ASCE)HY.1943-7900.0001516.**

Author keywords: Masonry bridge pier; Debris blockage; Scour; Laboratory experiments.

Introduction

Scour is widely recognized as the leading cause of bridge failures around the world (Chang 1973; HR Wallingford, and T. P. O'Sullivan & Partners 1991; Richardson et al. 1993; Parola et al. 1997; Melville and Coleman 2000; May et al. 2002; Hunt 2009; Ettema et al. 2010; Highways Agency 2012; Benn 2013; Toth 2015). There are several examples of scour-induced bridge failure just from the past decade: Bridge RDG1 48 near Feltham in England in 2009, Malahide Viaduct in Ireland in 2009, CPR Bonnybrook Bridge in Calgary, Canada, in 2013, I-10 Bridge in California in 2015, and several bridges in Cumbria, United Kingdom, that failed due to the floods of December 2015.

Experimental and computational research, particularly over the last few decades, have enhanced significantly the understanding of the scour process around bridge piers by describing the underpinning science, particularly of the flow field and the turbulent horseshow vortex (THV) system upstream of circular and rectangular piers (e.g., Melville and Coleman 2000; Kirkil et al. 2008; Escauriaza and Sotiropoulos 2011; Link et al. 2012; Apsilidis et al. 2015; Unsworth 2016; Bouratsis et al. 2017; Chen et al. 2017; Ettema et al. 2017).

A key factor widely acknowledged to increase the scour risk of bridges is debris blockage (Chang and Shen 1979; Diehl 1997; Parola 2000). Debris increases the effective width of a pier and constricts flow, thereby increasing streamwise and downward velocities at the pier (Laursen and Toch 1956; Melville and Dongol 1992), which in turn worsen scour (May et al. 2002; Bradley et al. 2005; McKibbins et al. 2006; Lagasse et al. 2010; Pagliara and Carnacina 2010; Wallerstein et al. 2010; Arneson et al. 2012; Benn 2013). The risk of debris blockage is particularly high for masonry bridge piers as they tend to be much wider than modern bridge piers (Hamill 1998; McKibbins et al. 2006). Their plan geometry is typically rectangular but with sharp or occasionally semicircular noses (cutwaters) that help streamline the pier. Masonry bridges constitute over 40% of the United Kingdom bridge stock (McKibbins et al. 2006), and are also common across Europe (Robinson 2000; Oliveira et al. 2010; Sarhosis et al. 2016). Also, a large number of these structures, particularly those built before 19th century (McKibbins et al. 2006), are classified as cultural and engineering heritage structures.

[1]Research Fellow, Centre for Water Systems, Univ. of Exeter, Devon EX4 4QF, UK (corresponding author). ORCID: https://orcid.org/0000-0003-3406-5526. Email: m.ebrahimi@exeter.ac.uk

[2]Senior Lecturer, College of Engineering, Mathematics and Physical Sciences, Univ. of Exeter, Devon EX4 4QF, UK. Email: p.kripakaran@exeter.ac.uk

[3]Professor, Faculty of Civil Engineering, Univ. of Belgrade, Belgrade 11000, Serbia. Email: dprodanovic@grf.bg.ac.rs

[4]Research Fellow, College of Engineering, Mathematics and Physical Sciences, Univ. of Exeter, Devon EX4 4QF, UK. Email: kah.recep@gmail.com

[5]Ph.D. Candidate, College of Engineering, Mathematics and Physical Sciences, Univ. of Exeter, Devon EX4 4QF, UK. Email: mjr214@exeter.ac.uk

[6]Associate Professor, College of Engineering, Mathematics and Physical Sciences, Univ. of Exeter, Devon EX4 4QF, UK. Email: g.r.tabor@exeter.ac.uk

[7]Professor, Institute for Infrastructure and Environment, Heriot-Watt Univ., Edinburgh EH14 4AS, UK. Email: s.arthur@hw.ac.uk

[8]Professor, Centre for Water Systems, Univ. of Exeter, Devon EX4 4QF, UK. Email: s.djordjevic@exeter.ac.uk

Note. This manuscript was submitted on September 25, 2017; approved on April 24, 2018; published online on September 22, 2018. Discussion period open until February 22, 2019; separate discussions must be submitted for individual papers. This paper is part of the ***Journal of Hydraulic Engineering***, © ASCE, ISSN 0733-9429.

Current literature on scour at bridge piers includes experimental work to understand the effect of debris blockage on flow and scour (Melville and Dongol 1992; Lagasse et al. 2010; Pagliara and Carnacina 2011a, b, 2013). However, it has two key limitations when examined particularly in the context of its usefulness for masonry bridges. First, previous research has focused primarily on circular and rectangular piers, which are common in modern steel and concrete bridges that constitute the highway network in most countries. The applicability of these results for masonry bridge piers, which have a sharp-nose geometry and a much larger streamwise length-to-width ratio than modern bridge piers, has not been investigated. Second, previous work has not captured adequately the relationship between local scour and debris elevation in the water column. Lagasse et al. (2010), which is the only study to consider the effect of debris elevation, used square piers. Other studies have typically assumed that debris is present just below the flow free surface, whereas in practice debris can be floating, partially submerged, or fully submerged.

This experimental study addresses directly the aforementioned two limitations and is thus novel in the following two aspects compared to previous experimental research. First, it characterizes the scour effects of debris blockage at sharp-nose piers. Second, it derives experimentally the relationship between debris elevation in water column and scour depth. Other novelties of this work include the following: It investigates debris-induced scour under shallow flow conditions, because bridge failures due to debris accumulation have been reported in nonflood conditions in small rivers. For example, Bridge RDG1 48 near Feltham in England (RAIB 2010) that failed due to debris blockage had a flow shallowness (flow depth to pier width) of 0.4 at the time of its collapse. Lastly, previous studies have focused on the maximum scour depth and have given less attention to evaluating the extent of scour and volume of scour hole with debris. This study is novel in its use of experimental data to derive a relationship between scour volume and maximum scour depth. This is of practical importance because debris is known to increase the spanwise extent of scour in addition to increasing scour depth, and hence helpful to calculate volume of the material required for filling scour hole in postflood remedial works.

This paper investigates the aforementioned aspects using clear-water scour experiments in a flume containing a scale model of a sharp-nose pier, with the flow angle of attack relative to the pier being zero. A length scale ratio of 1:10 is chosen to represent a small river having a width about 6 m, typical of those that are spanned by masonry bridges. Debris is modeled using stationary simplified geometries that extend only upstream of the pier.

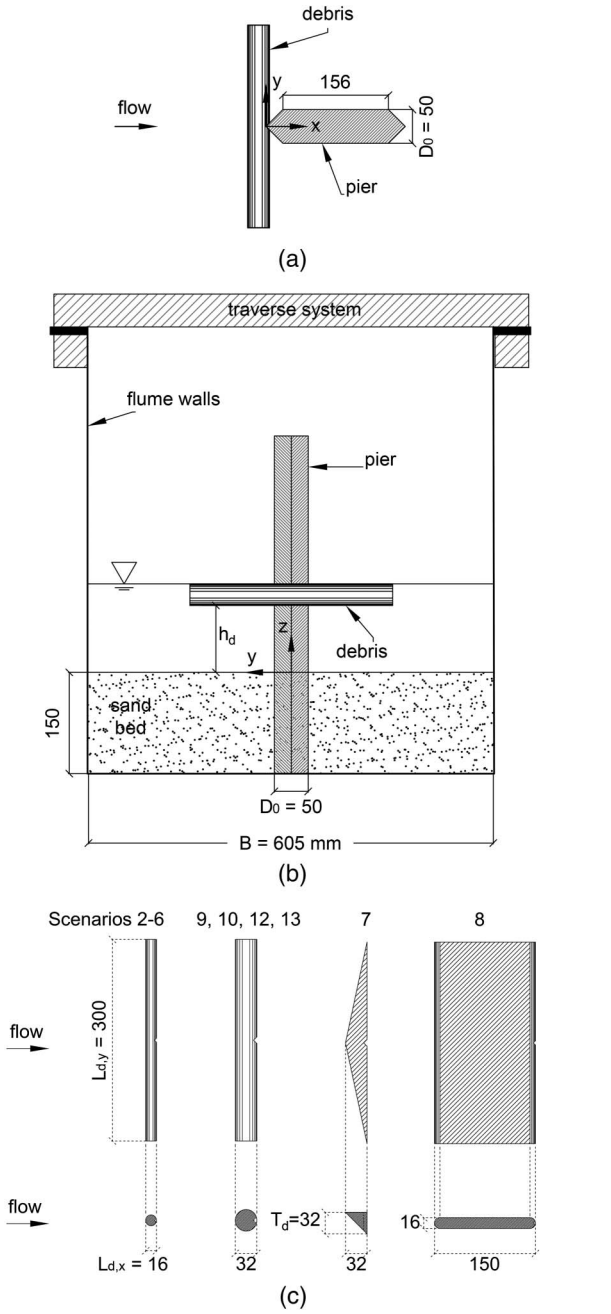

Fig. 1. (a) Schematic plan view of pier with fixed debris in Scenario 12; (b) looking downstream cross-sectional view in Scenario 12 (large cylindrical debris under FS); and (c) plan view (top, x–y plane) and side view (bottom, x–z plane) of debris shapes and dimensions used in the present work (Table 1): from left to right: small and large cylindrical (log shape), inverted-pyramid and plate debris; triangular notch on the debris midlength was used to fix debris perpendicular to the upstream nose of the pier. All dimensions are in millimeters.

Experimental Setup and Methodology

Flume

Experiments were carried out in a horizontal, 605-mm-wide, 10-m-long sediment recirculating flume at the University of Exeter, United Kingdom. The flume is equipped with a traverse system (with a movement precision of 1 μm) for positioning instruments at specified x, y, and z coordinates, where x, y, and z refer to streamwise, spanwise, and vertical directions as shown in Figs. 1(a and b). Experiments were started with a flat bed with $z = 0$ representing bed level at $t = 0$. The discharge was controlled with the aid of a variable-speed drive on the centrifugal pump driving the flow. Discharge was measured using an electromagnetic flowmeter (resolution ± 0.1 L/s) installed in the suction pipe of the water recirculating system. A digital point gauge mounted 3.5 m upstream of the pier was used to read the undisturbed elevation of free surface. The precision of this measurement was 0.5 mm due to free surface fluctuations.

Sand

Sediment was coarse, uniform silica sand with particle size d_{50}, uniformity coefficient d_{60}/d_{10}, and geometric standard deviation of sediment particle size distribution d_{84}/d_{50} equal to 1.37 mm,

1.37, and 1.21, respectively. This type of sand translates to medium gravel in prototype scale for the scaling ratio 1:10 chosen in this work. This choice of sediment was made to ensure

1. clear-water scour [with $U/U_{cr} = 0.94$, where U_{cr} = critical flow velocity for initiation of sediment movement, calculated as $U_{cr} = U/\eta_*^{1/2}$, where η_* = relative flow intensity calculated according to Yalin and da Silva (2001)];
2. rough turbulent flow ($\mathsf{R}_* > 70$, Yalin 1972); and
3. non–ripple-forming sand ($d_{50} > 0.6$–0.7 mm, Raudkivi and Ettema 1983; Ettema et al. 1998) to facilitate scour measurement.

The authors, however, acknowledge that the assumption of uniform bed material is rarely fulfilled in the field (Breusers et al. 1977; Melville and Sutherland 1988) because there is often a gradation of sediment. Consequently, the scour depths observed in field conditions are smaller than the depths predicted on the assumption of uniform bed material.

Pier

Geometry and dimensions of pier were defined according to available data on typical sharp-nose masonry bridge piers in the United Kingdom. As shown in schematic in Fig. 1(a), the pier featured wedge-shaped (triangular) cutwaters at its two noses. Each cutwater was an isosceles triangle with a base angle of 45°. Pier width was 50 mm, which is less than one-sixth of the width of the flume. This was chosen to minimize adverse effects of side walls, as recommended by Frostick et al. (2011). It also ensured that there will be no contraction scour according to the equation proposed by Richardson and Davies (2001). Streamwise length of the straight part of the pier was 156 mm, resulting in a width-to-length ratio of 0.32 that matches the average aspect ratio estimated for several masonry bridge piers in Devon, United Kingdom (Devon County Council, private communication, 2015–2017). The pier was fabricated out of PVC and fixed to the flume bed.

Debris

Various terms are used in the literature to refer to debris, e.g., log jam, debris raft, drift, and debris mass. While these terms can imply various debris geometries, they generally refer to accumulation of woody debris. In the present work, the process of debris accumulation, studied by Lyn et al. (2003) and Panici and de Almeida (2017), was not investigated. The latter investigated how debris dimensions vary with the Froude number of the characteristic length of individual debris elements. They found that the width to thickness of debris blockage is generally between 3 and 27. In this study, simplified debris shapes, with width-to-thickness ratios within the range found by Panici and de Almeida (2017), were considered. The shapes represented broadly the debris geometries observed to result from woody debris accumulation in full-scale scenarios. Specifically, four simplified debris shapes were used [Fig. 1(c)]. These included: (1) two cylindrical (log) shapes, (2) an inverted half-pyramid (triangular base), and (3) a plate. The cylindrical shapes represent tree trunks, which are the most common debris and can be the initiators for much larger debris mass (Diehl 1997). The inverted half-pyramid and plate shapes represent solid debris mass of small thickness, typical of debris pile-up. The inverted half-pyramid shape was chosen according to Wellwood and Fenwick (1990) and Diehl (1997), who identified a triangular-in-depth shape as one of the main geometries of debris accumulation. It is also similar to the debris shape used by Lagasse et al. (2010) and is a simplified version of the perfect inverted half-cone used by Panici and de Almeida (2017). The plate shape was chosen to represent a mat of small woody elements.

Debris was considered static for simplicity and fixed perpendicular to the pier at the desired elevation [Fig. 1(b)]. This was achieved by a 3 or 5-mm-deep 90° triangular notch at the mid-length of the debris. The dynamics of fluid–structure interaction between debris and flow was not studied due to the significant challenge in managing scaling issues, such as creating a debris model of suitable density. Also, understanding the influence of static debris on scour was an important first step to design the experiments that would be able to characterize the scour effect of the dynamics of debris.

Due to the large width and the elongated geometry of masonry bridge piers, debris seldom extends downstream in real-life bridges and was hence considered accordingly in the experiments. Also, all debris models used were solid and smooth as illustrated in Fig. 1(c). This is sufficient for the purposes of this study because, as found by Pagliara and Carnacina (2010) and Lagasse et al. (2010), porosity and roughness of debris do not affect depth and pattern of scour in any appreciable way and can only be considered secondary factors when compared with dimensions of debris and flow intensity.

The debris dimensions were chosen carefully considering real-life debris sizes and the experimental constraints. The spanwise length of debris, $L_{d,y}$, was expected to affect mainly the lateral (transverse) extent of scour and have minimal influence on the maximum scour depth (Lagasse et al. 2010). The value of $L_{d,y}$ was hence set to 300 mm for all debris shapes to maximize the lateral extent of scour while minimizing the effect of flume sidewalls. Diameter/length ratio of the smaller cylindrical debris was defined according to diameter/length ratio of tree debris observed in field conditions. Accordingly, this debris shape with diameter $T_d = 16$ mm had a diameter/length ratio $T_d/L_{d,y} = 0.059$, which is the average diameter/length ratio of trees suggested in several field surveys of woody debris in the United States and Europe (Beechie and Sibley 1997; Diehl 1997; Kail 2003; Comiti et al. 2006; Magilligan et al. 2008). The second cylindrical debris with diameter $T_d = 32$ mm was used to quantify the relationship between diameter of the debris and scour. The inverted half-pyramid debris had the same thickness and streamwise length as the large cylindrical debris. This was done to enable comparison between scour maps generated by the two geometries. The plate debris had a thickness of 16 mm and a streamwise length of 150 mm.

The debris models were either 3D-printed or made from steel. The cylindrical shapes and the inverted half-pyramid shape were represented using 3D-printed nylon objects. Steel was used to fabricate the plate geometry as well as a second model of the smaller cylindrical debris. This was aimed specifically at investigating the influence of the streamwise length of resting-on-bed debris on scour.

Hydraulic Conditions of Experiments

Hydraulic conditions of experiments are presented in Table 1. Here, D_0 = pier width; B = width of approach flow (= flume width); h = depth of approach flow; Q = flow discharge; R = flow Reynolds number $\{=Uh/\nu$, with U and ν being mean velocity of approach flow $[=Q/(Bh)]$ and fluid kinematic viscosity, respectively$\}$; F = Froude number $\{=U/(gh)^{1/2}$, where g stands for acceleration due to gravity$\}$; R_* = roughness Reynolds number $[=u_*k_s/\nu$ with u_* = shear velocity calculated as proposed by Sheppard et al. (2014), and k_s = granular roughness = $2d_{50}$ (Kamphuis 1974), where d_{50} is median particle size of sand]. The term d_s is the maximum measured scour depth.

The experiments were performed for two flow depths, $h = 80$ and 131 mm, each with corresponding discharges $Q = 19.1$ and 33.4 L/s, respectively. For each experiment, the approach flow

Table 1. Hydraulic conditions and characteristics of scour experiments

Scenario	Approach flow depth $h \pm 0.5$ mm	Discharge $Q \pm 0.1$ L/s	R	F	R_*	Debris shape	Position in water column of debris	Streamwise length of debris $L_{d,x}$ (mm)	Spanwise length of debris $L_{d,y}$ (mm)	Thickness or diameter of debris T_d (mm)	Maximum scour depth $d_s \pm 1$ mm
1	80	19.1	31,570	0.45	76.6	No debris	—	—	—	—	78.3
2						Cylindrical	Under FS	16	300	16	88.9
3						Cylindrical	Mid depth	16	300	16	82.9
4						Cylindrical	Near bed	16	300	16	79.3
5						Cylindrical	Fixed on bed	16	300	16	68.8
6						Cylindrical	Resting on bed	16	300	16	58.2
7						Inverted pyramid	Under FS	32	300	32	87.2
8						Plate	Resting on bed	150	300	16	48.7
9						Cylindrical	Under FS	32	300	32	104
10						Cylindrical	Fixed on bed	32	300	32	83.4
11	131	33.4	55,207	0.37	77.5	No debris	—	—	—	—	85.4
12						Cylindrical	Under FS	32	300	32	110
13						Cylindrical	Fixed on bed	32	300	32	80.3

Note: $d_{50} = 1.37$ mm; $D_0 = 50$ mm; and $B = 605$ mm.

depth, discharge, and debris distance from the initial bed were adjusted carefully to within 0.5 mm, 0.1 L/s, and 0.5 mm, respectively, of the desired values. Reynolds number scaling was not strictly adhered to but R was kept between 31,000 and 55,000 to ensure the flow was turbulent (Chanson 2004) in all the scenarios. In addition, approach flow was also kept subcritical (F < 1). Flow shallowness, h/D_0, was 1.6 and 2.6 for the two flow depths, corresponding to shallow flow conditions (Chiew 1992; Melville and Chiew 1999). The value $h/D_0 = 1.6$ was the smallest feasible value that could be attained under the experimental constraints; $h/D_0 = 2.6$ was smaller than the flow shallowness used in most of the previous research (Lagasse et al. 2010; Pagliara and Carnacina 2011b).

Measurements

Each scour experiment lasted 5 hours (300 min), which at $U/U_{cr} = 0.94$ results in the scour depth reaching about 87% of the equilibrium scour depth for a circular pier without debris (Melville and Chiew 1999). This was deemed sufficient for the following two reasons. First, the purpose of this research was to quantify the effect of various debris shapes and their elevations on scour depth and volume. To achieve this, running all experiments for identical but reasonable durations that led to quasi-equilibrium scour depth is sufficient. At quasi-equilibrium state, sand particles are not dislodged by the flow but a few of them have rolling motion which does not change scour depth noticeably (Dey 1995). This was proved by visual observations during the experiments and is evidenced by the upstream slope of scour hole being larger than repose angle of sand as discussed in the section "Results and Discussion". Second, the duration of 5 h at present lab scale (1:10) is equivalent to $5 \times 10^{0.5} = 15.8$ h in prototype conditions, which represents a flood of significantly long duration for a small river as considered here. In fact, many researchers (e.g., Melville and Chiew 1999) have stated that scour predictions based on experiments that are run until equilibrium scour depth is attained can be overly conservative, because real flood events are generally of much shorter durations.

In each scour experiment, only the final scour profile (after 5 h) was measured. This was carried out after stopping the flow very gradually and removing debris. Scour topography was mapped by measuring distances from the bed on a grid of approximately 250 (x, y) points. This was carried out using an echo sounder that was built into the Nortek Vectrino Profiler mounted on the traverse system of the flume. The echo sounder used the time of flight of an acoustic signal to measure the distance to the bed and had an advertized accuracy of 0.5 mm. Scour depth at the points close to the boundary of the pier that could not be measured using the echo sounder were measured manually, with precision of 0.5 mm, using a digital point gauge. Measurements were typically taken on only one side of the pier due to the symmetry in scour profile about the x–z plane. The symmetry was verified for Scenarios 9 and 10 using scour measurements taken on both sides of the pier. Fig. 2, where red and green shades show erosion and deposition, respectively, illustrates the almost perfect symmetry in scour maps in the vicinity of the pier for the two scenarios. Additionally, symmetry in scour topography was also checked visually for each experiment. The repeatability of the experiments was confirmed by comparing the maximum scour depth and overall scour pattern obtained after 5 h over two runs for a few scenarios. A final map of scour to an accuracy of ±1 mm was produced by combining all the measured points.

Results and Discussion

Scour Map

Contour maps of scour for the measured half of the flume for all scenarios are illustrated in Fig. 3. The location of maximum scour depth, d_s, is shown by an enhanced dot on the pier cutwater. In most experiments, this was located at the corner of cutwater with $x = 25$ mm and $y = -25$ mm. This finding is in agreement with results obtained for similar sharp-nose piers without debris in 2-h experiments by Müller et al. (2001) and 8-h experiments by Vijayasree et al. (2017). Khosronejad et al. (2012) also obtained similar results for diamond piers through flume experiments and numerical simulations that were run until equilibrium scour was reached. This finding differs markedly from observations for rectangular/circular piers for which the maximum scour depth d_s is seen to occur at the upstream face of the pier (e.g., Melville 1975; Breusers et al. 1977; Lagasse et al. 2010). The different locations of maximum scour depth for rectangular/circular piers and sharp-nose piers may be due to the following two factors related to the flow around the pier: First, the turbulent horseshoe

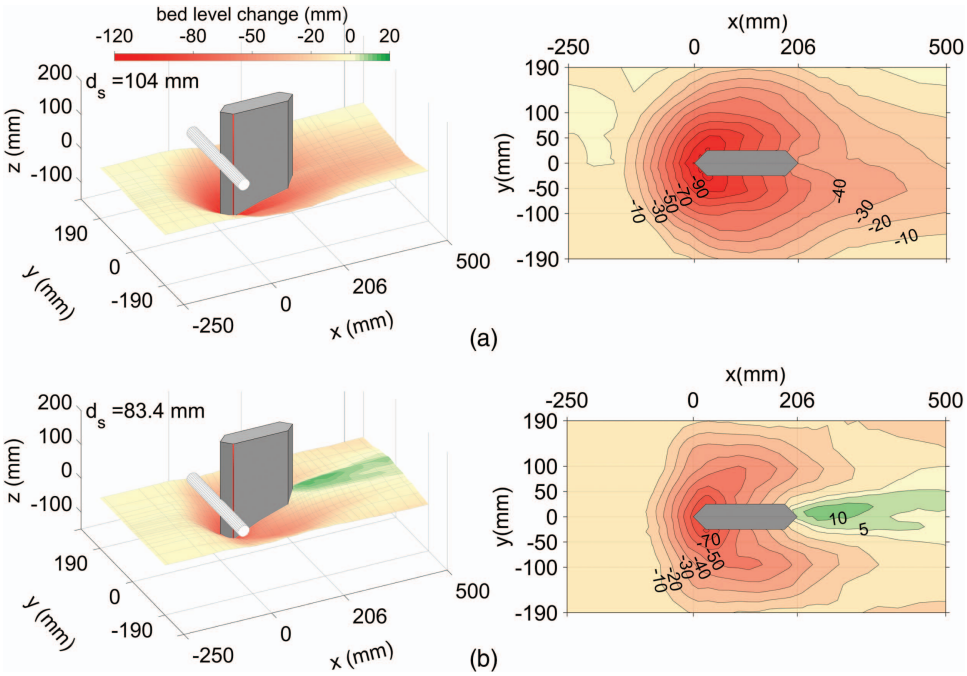

Fig. 2. (Color) Three-dimesnional and contour maps of scour for scenarios: (a) 9; and (b) 10. Red line marks location of maximum depth of scour d_s. The cylindrical (log shape) object is the solid debris which was removed before scour measurements.

vortex (THV) system, which is known to be the primary factor causing scour at the upstream face of rectangular/circular piers (Kirkil et al. 2008; Escauriaza and Sotiropoulos 2011; Link et al. 2012; Apsilidis et al. 2015; Bouratsis et al. 2017; Chen et al. 2017), has been observed by previous researchers (Shen et al. 1966; Breusers et al. 1977) to be not as well pronounced at the leading edge of sharp-nose piers. Second, the flow separation and the shedding of the two shear-layers at the two side corners of a sharp-nose pier increases bed shear stresses at these corners (Khosronejad et al. 2012; Vijayasree et al. 2017) and may thereby lead to maximum scour occurring at these locations. In Scenarios 5 and 6, the maximum scour depth occurred between the upstream nose of the pier and lateral corner of cutwater at $x = 12.5$ mm. However, the maximum scour depths in these two scenarios were only 0.5 and 1.4 mm larger than the scour depths observed at the corner of the cutwater.

The contour plots and the d_s values for Scenarios 5, 6, 8, 10, and 13 show that debris had a protective effect when on the bed which reduced maximum scour depth. Due to this, the shapes (in plan) of the scour holes for these scenarios differ from the overall shape observed for other scenarios in Fig. 3.

In experiments with $h = 80$ mm, d_s increased from 78.3 mm in Scenario 1 without debris to 88.9 and 104 mm in Scenarios 2 and 9 that used 16 and 32-mm cylindrical debris respectively. This corresponds to 14% and 33% increase in d_s. For $h = 131$ mm, d_s increased from 85.4 mm in Scenario 11 without debris to 110 mm in Scenario 12 with 32-mm cylindrical debris, i.e., 29% increase. Also, d_s for Scenarios 2 and 9 is greater than that for Scenario 11 for which flow depth is comparatively much larger. This shows that the presence of debris in shallow flow ($h/D_0 = 1.6$) can lead to scour depths exceeding those due to deep flow ($h/D_0 = 2.6$) without debris, as can be also inferred from Melville and Dongol (1992) for a circular pier. By keeping debris dimensions constant, flow area reduction will be higher in shallow flow compared to deep flow. Therefore, under-free-surface debris will increase velocities (both streamwise and vertical) and, therefore, bed shear stress and consequently scour depth. Similarly, by keeping flow depth constant, thicker and under-free-surface debris increases velocities, bed shear stress, and scour depth more than a thin debris. This result has important implications for scour management of bridges as it highlights the importance of monitoring debris accumulation even when flow is shallow, such as when there may be no flooding. A real-life example of a bridge failure under shallow flow conditions may be Bridge RDG1 48 near Feltham in England, which failed due to scour-induced subsidence in November 2009. The United Kingdom's Rail Accident Investigation Branch, in its post-event investigation report, had noted that substantial scour had occurred despite flow depth being below the level for a flood alert, and that this was most likely due to debris accumulation that was observed upstream of the subsided abutment (RAIB 2010).

Another finding from the contour maps is that the maximum scour depth d_s for Scenario 7 was 16% smaller than that for Scenario 9. The overall size of scour hole for Scenario 9 was also larger than that for Scenario 7. This can be attributed to the fact that the inverted-pyramid debris has a smaller blockage area in the plane normal to the flow (i.e., in y–z plane) than the cylindrical debris. Consequently, the inverted-pyramid debris may have caused a smaller increase in flow velocities and bed shear stress than the cylindrical debris of identical thickness.

As can be inferred from Fig. 3, the presence of debris just under the flow free surface (Scenarios 2, 7, 9, and 12) caused maximum scour. For these scenarios, the effect of debris on flow can be qualitatively explained as follows. Debris at the pier reduced flow cross-sectional area. Reduced flow area led to acceleration of the flow and increased bed shear stress. Also, when debris was located just under the flow free surface, it diverted flow streamlines towards the bed, thereby increasing downward flow which loosens and lifts sediment particles (e.g., Hjulstrom 1939; Shen et al. 1966; Yalin 1972; Melville 1975; van Rijn 1993). Together these two phenomena increased sediment transport and hence enhanced scour around the base of the pier. At the beginning of the experiments, the onset of scour was observed at the upstream nose of the pier, possibly due

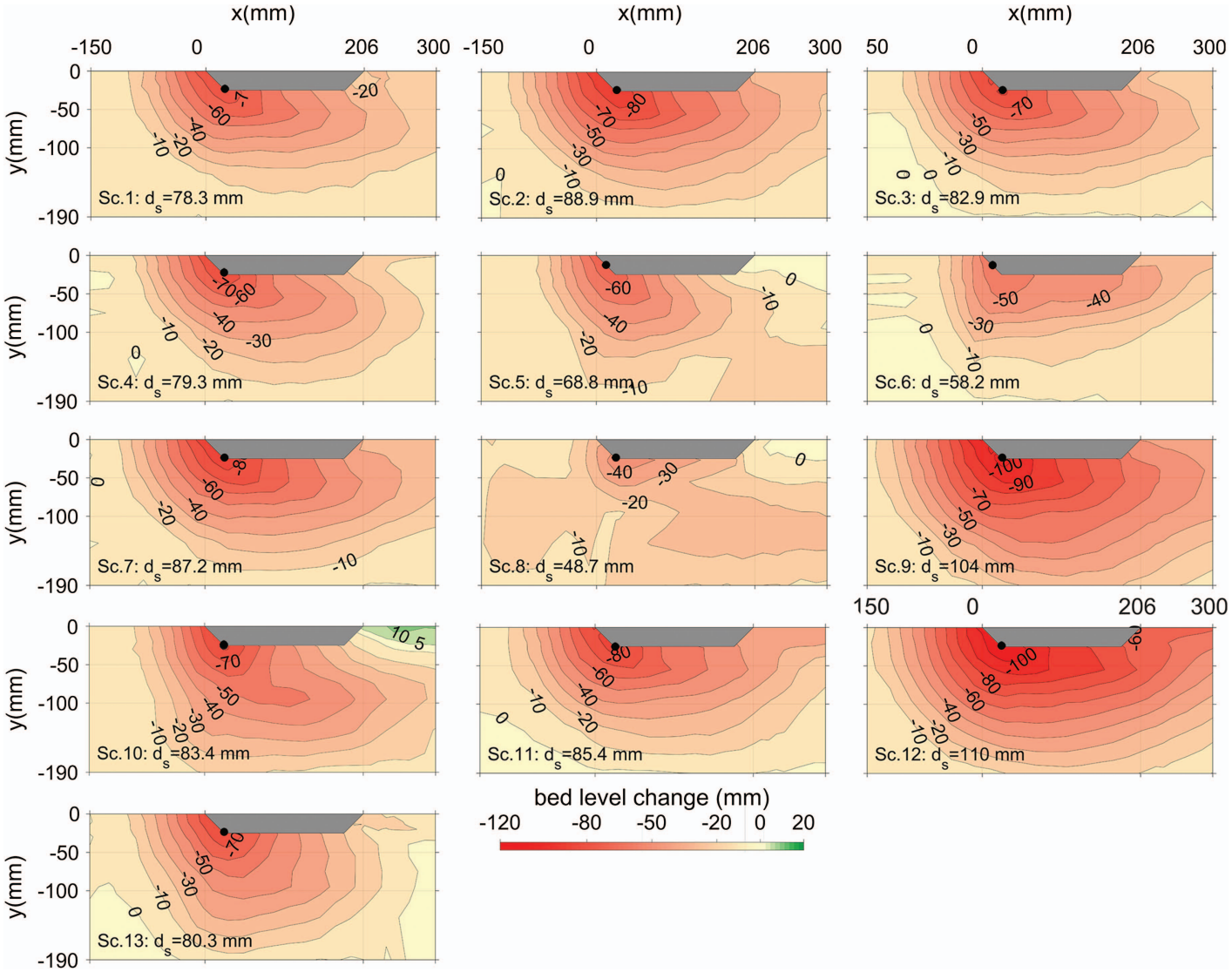

Fig. 3. (Color) Contour maps in the measured half of the flume width for all scenarios. Sc.# is the scenario number. Gray solid area represents the pier. Enhanced dots on the pier marks location of maximum scour depth d_s.

to the presence of a horseshoe vortex. However, as the scour progressed, downflow at the pier base was forced into the scour hole by the three-dimensional vortex generated by flow separation from the bed at the upstream edge of scour hole (Dey et al. 1995). This caused scour to quickly propagate downstream where vortex shedding from the two upstream lateral corners of the pier would further increase scour depth.

A simple but approximate way of determining the scour due to debris in front of a pier is to superimpose the scour depths produced individually by the pier and the debris. Debris can be considered to create a pressurized flow as during inundation of bridge decks proposed by Umbrell et al. (1998). The continuity of flow discharge necessitates that total flow discharge, Q, at location of debris can be split as follows:

$$Q = Q_{\text{above}} + Q_{\text{below}} \tag{1}$$

where Q_{above} and Q_{below} = discharges passing above and below debris, respectively. For ease of computation, the mean flow velocity above debris can be assumed to be equal to the mean approach velocity, and the mean flow velocity below debris, at equilibrium stage of scour, can be assumed to be equal to the critical velocity. Then

$$UhB = Uh_aB + U_{cr}(h_d + d_{s,p})B \tag{2}$$

where h_a and h_d = height of approach flow above and below debris; and $d_{s,p}$ = scour depth due to pressurized flow. Rearranging Eq. (2) gives

$$d_{s,p} = \frac{U}{U_{cr}}(h - h_a) - h_d \tag{3}$$

When debris is located just under flow free surface, i.e., for Scenarios 2, 9, and 12, with $h_a = 0$ and $h_d = 64$, 48, and 99 mm, Eq. (3) yields $d_{s,p} = 11.2$, 27.2, 24.1 mm, respectively. Therefore, the total scour depths, i.e., $(d_{s,p} + d_{s,0})$ where $d_{s,0}$ is the scour depth for the scenario without debris, are 89.5, 105.5, and 109.5 mm, respectively. These values are within $\pm 1.5\%$ of the measured values. It is worthwhile to mention that this approach did not predict the measured scour depths for scenarios with debris being at elevations other than just under the flow free surface.

This can be due to the complexity that debris at lower elevation introduces into the flow and sediment transport.

Extension and Volume of Scour around Pier

Figs. 4(a and b) show longitudinal and cross-stream profiles of scour at x–z and y–z planes passing through $y = -26.1$ and $x = 25$ mm respectively. These x and y coordinates correspond to the scour measurement point nearest to the lateral corner of the pier cutwater, where the maximum scour depth was observed for most of experiments (Fig. 3). The upstream slope of the scour hole along x in all experiments was ~32° [Fig. 4(a)], which is 23% higher than the angle of repose for the chosen sand. This demonstrates that, while equilibrium scour depth may not have been reached, the 5-h duration of the experiments was sufficient to attain quasi-equilibrium scour as defined by Dey et al. (1995). Also, while in some scenarios (e.g., 9 and 10) the scour hole was seen to extend toward the flume side walls [Fig. 4(b)], there was no actual scour observed visually at the walls. This can also be approximately verified using the measured scour data. For example, for Scenario 9 in Fig. 4(b), the bed elevation at $y = -190$ mm was -16.9 mm. As the scour profile has an approximately constant gradient towards the flume wall ($y = -302.5$ mm), then the point where there is no scour ($z = 0$) is at $y \simeq -226$ mm, which is 76 mm away from the flume wall. This implies that there was no contraction scour in the experiment, which is also verified by the equation proposed by Richardson and Davies (2001).

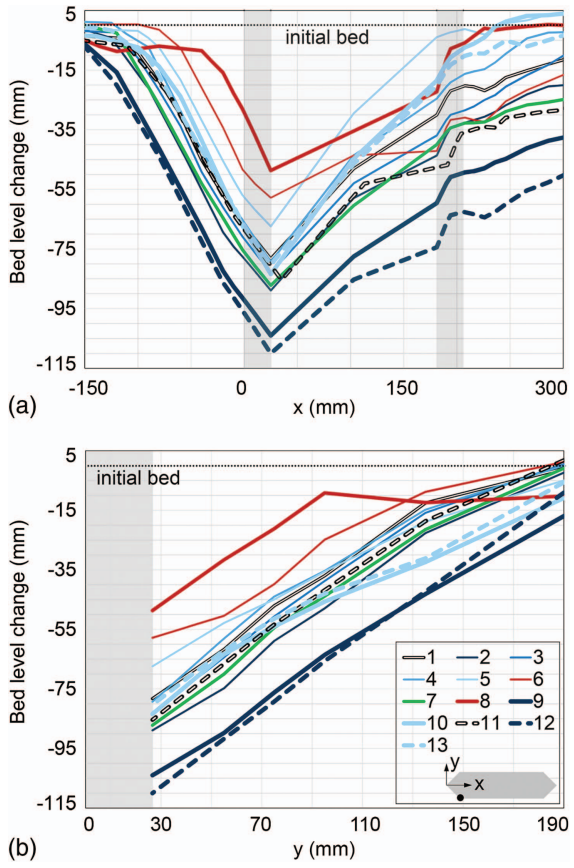

Fig. 4. (Color) Profiles of scour close to the lateral corner of cutwater (i.e., close to location of maximum scour depth shown by a dot in the insert): (a) streamwise profiles at $y = 26.1$ mm; and (b) cross-stream profiles at $x = 25$ mm. Gray area represents the pier.

As can be seen in Fig. 4, both streamwise and cross-stream extent of scour generally increased with d_s. The exceptions are Scenarios 6 and 8 (red plots) where debris was resting on the initial bed and could move downward as scour progressed. This caused the shape of the scour hole to deviate from those for the rest of scenarios. In Scenarios 2–5, d_s and streamwise extent of scour decreased with debris elevation. Spanwise extent of scour however changed negligibly. This is due to the use of the same spanwise length $L_{d,y}$ for all debris models.

The longitudinal extent of scour in Scenario 6 was significantly greater than that for Scenario 5 even though both scenarios used identical debris dimensions. This is due to the debris being fixed at its elevation in Scenario 5, which diverted the flow under debris and toward the bed. This meant flow energy was dissipated mainly via increasing d_s and not extending scour downstream. In Scenario 6, because debris was resting on the bed and moved downward as scour progressed, it protected the bed to a degree and diverted the flow over which caused downstream extension of scour. In Scenario 8, the plate debris protected the bed in all three directions by diverting the flow away from the bed and caused very little longitudinal and spanwise extent of scour. Some small secondary scour was however observed adjacent to the plate edges parallel to the flow direction.

The volume of the scour hole V_s, which is indicative of the extent of loss of soil support to the pier foundation, was calculated for each scenario using the scour map for the hatched region around the pier shown in the schematic insert of Fig. 8. The value of V_s is observed to increase from 1.45 L for Scenario 1 without debris to 1.8 and 2.7 L for Scenarios 2 and 9, respectively, with cylindrical debris. These values indicate 24% and 86% increase in V_s for an increase of 14% and 33% respectively in maximum scour depth d_s. Also, a 100% increase in debris thickness from Scenario 2 ($T_d/h = 0.2$) to Scenario 9 ($T_d/h = 0.4$) caused a 50% increase in scour volume.

As the streamwise and spanwise extents of scour increase with d_s, the total volume of scour hole, V_s, is also expected to increase with d_s. The exact nature of the relationship between d_s and V_s is found by fitting an equation to the data as shown in Fig. 5. The volume of scour is seen to increase quadratically with d_s following the equation $V_s = 0.00022d_s^2$, where V_s and d_s are in liters and millimeters, respectively. In prototype scale, the corresponding equation will be $V_s = 2.2d_s^2$, where V_s and d_s are in cubic meters and meters, respectively. This equation has a similar form to equations proposed by Link et al. (2008) and Diab et al. (2010)

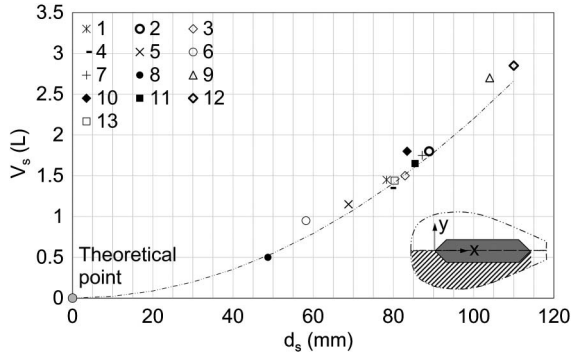

Fig. 5. Volume of truncated scour hole (hatched zone) calculated at one side of the flume up to the downstream nose of the pier; dash curve is a quadratic curve ($V_s = 0.00022d_s^2$; V_s and d_s are in liters and millimeters, respectively) fitted over the data.

for scour at circular and square piers in the absence of debris. This information can be useful in planning post flood remedial works (e.g., Solaimani et al. 2017) where often only maximum scour depth is initially measured.

Effect of Debris Elevation

The effect of debris elevation on maximum scour depth was investigated using the cylindrical shapes (Table 1). Fig. 6 shows the variation of normalized scour depth ($d_s/d_{s,0}$) versus normalized debris elevation (h_d/h) as derived from measured data. The term $d_{s,0}$ is the scour depth observed for the related baseline scenario, i.e., when there is no debris. The term h_d is debris elevation as measured from the initial bed level to the bottom of the debris; $h_d/h = 0$ corresponds to scenarios where the bottom of debris was at the initial bed level; and $h_d/h = 1$ corresponds to scenarios where the debris is just above the free surface of approach flow (i.e., equivalent to no debris). Data for Scenarios 1–5, with $h/D_0 = 1.6$ and $T_d/h = 0.2$, are shown using squares. As can be inferred from the figure, scour was maximum when debris was located just below the free surface, i.e., for Scenario 2 with $h_d/h = 0.8$. The scour depth reduced as debris was moved downwards. This relationship between debris elevation and scour depth can be explained as follows. When debris is just below the free surface, it diverts the streamlines below it downwards toward the bed and a large portion of flow impacts the bed. However, as debris is moved closer to the bed, it splits the flow and only those streamlines obstructed by the debris or below it are directed downward. The rest of the streamlines are above the debris and cannot affect the bed significantly. The streamlines below debris impact the bed but because their velocities are smaller than those close to the free surface, the scour depths they produce also reduce with debris elevation. Lastly, when debris rests on the bed, it protects the bed to a large extent as most of the flow has to pass over the debris. In addition, and compared to the case with debris just under the flow free surface, scour depth reduced if the debris was removed from the flow. These results confirm the overall pattern observed by Lagasse et al. (2010).

Because the characteristics of the physical process of scour were not expected to change with cylindrical debris diameter and flow depth, fewer scenarios were explored for cylindrical debris of 32-mm diameter at $h = 80$ and $h = 131$ mm. The purpose was to understand how the maximum scour depth varied assuming the overall nature of the relationship between $d_s/d_{s,0}$ and h_d/h remains unchanged. Results for Scenarios 1, 9, and 10 with $h/D_0 = 1.6$ and $T_d/h = 0.40$ and for Scenarios 11, 12, and 13 with $h/D_0 = 2.6$ and $T_d/h = 0.24$ are also shown in Fig. 6. These two latter curves further confirm an earlier observation that debris accumulation in shallower flow can cause scour depths that exceed those during deep flow without debris.

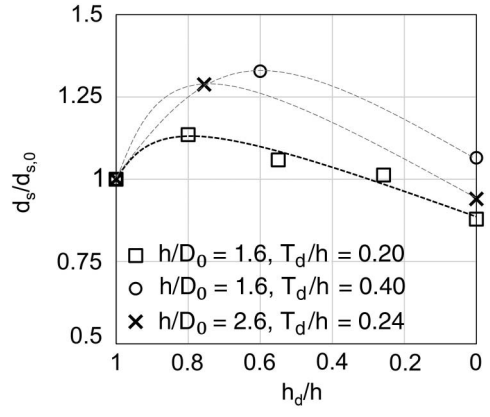

Fig. 6. Normalized scour depth $d_s/d_{s,0}$ (with respect to the corresponding baseline, no-debris scenario) versus normalized elevation of debris h_d/h for cylindrical (log shape) debris with $T_d/h = 0.20$ (Scenarios 1–5), $T_d/h = 0.40$ (Scenarios 1, 9, and 10), and $T_d/h = 0.24$ (Scenarios 11–13).

Effect of Debris Streamwise Length

Scour results for Scenarios 1, 6, and 8, in which debris was resting on the bed and only streamwise length of debris $L_{d,x}$ was changed, can be used to characterize the influence of streamwise length of resting-on-bed debris on scour depth. Similar to this analysis, scour depth d_s and streamwise length of debris $L_{d,x}$ are normalized with respect to $d_{s,0}$ and h, respectively. Here $d_{s,0}$ corresponds to the scour depth for the related no-debris scenario, i.e., Scenario 1 with $L_{d,x} = 0$. The normalized quantities are plotted in Fig. 7. The protective effect of debris is seen to increase with increasing $L_{d,x}$. However, after $L_{d,x}/\mathrm{h} \simeq 1.8$, further increment of $L_{d,x}$ does not affect scour significantly because there is always some scour just downstream of debris.

The results indicate that debris resting on bed can reduce scour depth by around 50% relative to the scour depth for no-debris scenario ($d_s/d_{s,0} \sim 0.5$). This is in contrast to the scour worsening effects of debris, when it is just under the flow free surface shown previously. In fact, for this scenario (i.e., $h_d = h$), Lagasse et al. (2010) and Pagliara and Carnacina (2011a) found that maximum scour occurs when streamwise length of debris is equal to flow depth and $3D_0$, respectively.

Effect of Debris Thickness

Based on the scour depths in Scenarios 1, 2, and 9, and data from Melville and Dongol (1992), Lagasse et al. (2010), and Pagliara and Carnacina (2011b) an attempt is made to characterize the influence of debris thickness T_d on scour depth. Data from each of the four sources that have identical hydraulic conditions and debris characteristics excluding T_d are grouped together. Groups that have at least three data points are considered in this analysis. Only debris with a rectangular cross-section section in the plane normal to the flow (i.e., y–z plane) is investigated here. Scour depth and debris thickness are presented in normalized form, i.e., $d_s/d_{s,0}$ and T_d/h in Fig. 8. Two exponential curves were fitted to data; $d_s/d_{s,0} = 1 + 3.2(T_d/h)^{1.237}$ for data from Pagliara and Carnacina (2011b) and $d_s/d_{s,0} = 1 + 0.32(T_d/h)^{1.237}$ for the rest of data.

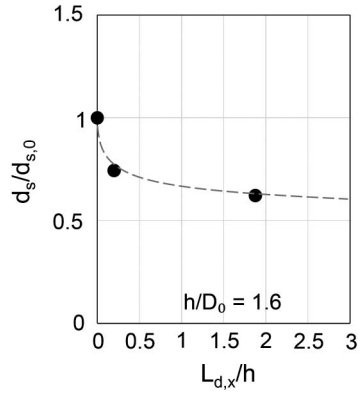

Fig. 7. Normalized scour depth $d_s/d_{s,0}$ versus normalized streamwise length of debris $L_{d,x}/h$ for Scenarios 1, 6, and 8.

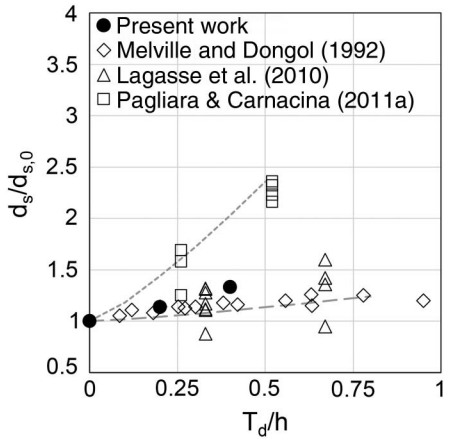

Fig. 8. Normalized scour depth $d_s/d_{s,0}$ versus normalized thickness of debris T_d/h for Scenarios 1, 2, and 9 of the present work and data from Melville and Dongol (1992), Lagasse et al. (2010), and Pagliara and Carnacina (2011b). Coarse and fine dash lines with equations $d_s/d_{s,0} = 1 + 0.32(T_d/h)^{1.237}$ and $d_s/d_{s,0} = 1 + 3.2(T_d/h)^{1.237}$ show exponential curves for scour depth increasing with debris thickness.

The general form of the equation is adopted from an extensive study by Pagliara and Carnacina (2011b), with a new coefficient and exponent derived to minimize differences with measured values. The value of $d_s/d_{s,0}$ increases from 1 for $T_d/h = 0$ (Scenario 1) to 1.04 for $T_d/h = 0.2$ (Scenario 2) and then to 1.1 for $T_d/h = 0.4$ (Scenario 9).

Scour Prediction with Widely Used Equations

The performance of the following four widely used equations for estimation of maximum scour depth is compared using the collected data:

1. Melville and Chiew (1999),
2. Richardson and Davies (2001),
3. Oliveto and Hager (2002), and
4. Sheppard et al. (2014).

All these equations were developed solely for a pier-only case and were not intended for estimating scour due to debris blockage. However, due to the lack of an approach that explicitly accounts for debris effects, these equations are still used by practitioners for estimating debris-induced scour by using the equivalent pier width concept proposed by Melville and Dongol (1992) and Lagasse et al. (2010). In this section, the experimental results are used to compare the performance of the equations when using the equivalent pier width approach.

To account for the sharp-nose geometry of the pier, a shape factor of 0.9 was applied to the original width of pier D_0 as recommended by Melville (1997) and Richardson and Davies (2001). Also, chosen equations, except that of Oliveto and Hager (2002), calculate equilibrium scour depth while the laboratory data were collected after 5 h. To enable comparisons with the measured scour depth, the equilibrium scour depth predicted by each equation was converted to scour depth at $t = 300$ min using the equation for temporal development of scour proposed by Melville and Chiew (1999).

Results from the equations were only analyzed for scenarios with debris located just under the free surface, i.e., Scenarios 1, 2, 7, 9, 11, and 12. For cases with debris, an equivalent pier width D_e was evaluated to account for the effect of debris blockage. The value of D_e was estimated using the equations by Melville and Dongol (1992), and its modified version proposed by Lagasse et al. (2010) (Table 2). For each scenario, measured scour depth d_s was compared to the estimated scour depth from each equation $d_{s,EST}$ [Figs. 9(a and b)]. Also, the mean percentage error relative to the measured value was calculated for each equation (Table 3). From Figs. 9(a and b), and Table 3, it is clear that the equation by Richardson and Davies (2001) consistently resulted in estimations closest to the measured values compared to the other three equations. The equation by Oliveto and Hager (2002) was observed to underestimate scour. The equations by Melville and Chiew (1999) and Sheppard et al. (2014) were seen to overestimate scour and may hence be preferred for design purposes in cases in which a degree of conservatism is sought.

Table 2. Equivalent pier width D_e (mm) calculated from equations proposed by Melville and Dongol (1992) and Lagasse et al. (2010)

Scenario	Melville and Dongol (1992)	Lagasse et al. (2010)
1	50	50
2	76	69.5
7	—[a]	64
9	102	89
11	50	50
12	81.8	73.8

[a]Equation of Melville and Dongol (1992) does not apply to this case with nonrectangular debris in profile.

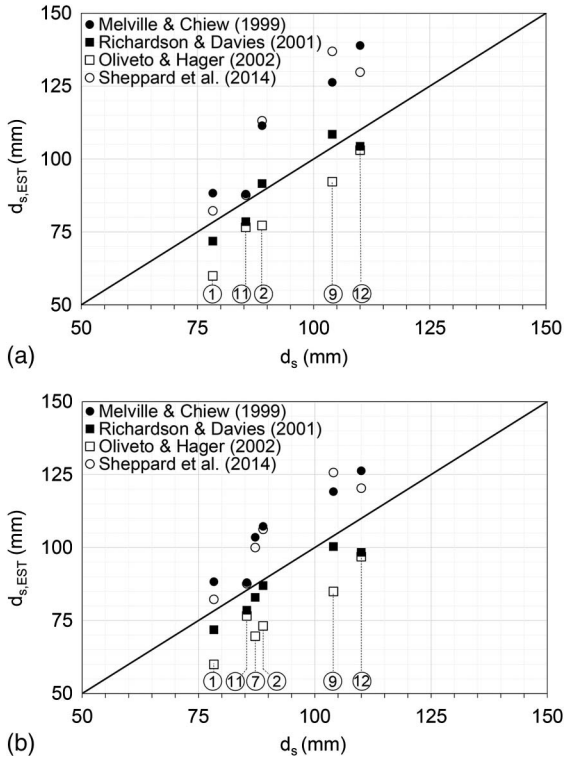

Fig. 9. Estimated depth of scour $d_{s,EST}$ from four equations versus measured depth of scour d_s in experiments with debris under free surface. Equivalent pier width (listed in Table 2) was calculated using: (a) Melville and Dongol (1992); and (b) Lagasse et al. (2010). Points along each vertical line are for the scenario whose number is shown in a circle.

Table 3. Mean difference (%) of scour depth estimated using chosen equation, $d_{s,EST}$, and measured scour depth d_s

Reference	Equivalent pier width D_e calculated using	
	Melville and Dongol (1992)	Lagasse et al. (2010)
Melville and Chiew (1999)	17.6	13.2
Richardson and Davies (2001)	−1.2	−6.5
Oliveto and Hager (2002)	−14.3	−16.3
Sheppard et al. (2014)	18.8	11.5

Conclusions

This paper presents findings from flume experiments on a sharp-nose pier with simplified debris shapes. The main conclusions from this work are as follows.

1. The 5-h experiments in this study represented a short-duration flood event in prototype scale. For this scenario, maximum measured scour depth for the sharp-nose pier was located at the lateral corners of the pier cutwater or in between the upstream nose of pier and lateral corner of cutwater. This agrees with available literature for sharp-nose piers and is different from that of circular and rectangular piers for which maximum scour is at the upstream nose of the pier. This can help postflood inspection works for identifying the maximum scour depth.
2. Scour depth was measured in shallow flow conditions with $h/D = 1.6$ and 2.6. This increase in flow shallowness resulted in 9% increase in maximum scour depth. Change of scour depth due to debris was also measured. It was found that cylindrical debris (being just under the flow free surface) enhanced scour, compared to no-debris case, by 33% and 29% for the values of flow shallowness, respectively. It is also worthwhile to note that scour depth in shallower flow with large-log debris was higher than that of deeper flow without debris (Fig. 6). This highlights the importance of monitoring debris build-up in field conditions even when flow is shallow and water levels may be well below flood conditions.
3. The longitudinal and lateral extents of scour are observed to increase with scour depth (Fig. 4). The volume of scour hole was found to increase quadratically with maximum scour depth measured after 5 h (Fig. 5). This trend is similar to what was found in previous research for scenarios without debris. The proposed equation can be useful for calculating the volume of material required for filling scour holes in postflood remedial field works in which only maximum scour depth is measured.
4. At a sharp-nose bridge pier, debris had the maximum scour enhancing effect when it was located just under the flow free surface (Fig. 6). This agrees with findings by previous researchers for rectangular piers. This study also investigated in detail the variation of scour depth with debris elevation. As debris moved closer to the bed, scour depth decreased. The least scour was observed when debris was resting on the bed. In fact, cylindrical debris was found to protect the bed to some extent and reduce maximum scour depth to nearly the same as the case without debris. The increase of debris length in streamwise direction, up to about $1.8h$, can protect the bed and reduce the scour depth by around 50% relative to no-debris conditions. Further increase of debris length does not affect scour (Fig. 7).
5. Among the four equations for scour estimation that were evaluated, the CSU equation (Richardson and Davies 2001) outperformed other equations and was least conservative. The equation by Oliveto and Hager (2002) was found to underestimate scour while equations by Melville and Chiew (1999) and Sheppard et al. (2014) overestimated scour and may be preferred for design purposes in cases in which a degree of conservatism is sought.

Acknowledgments

The research presented in this paper was supported by funding from the United Kingdom's Engineering and Physical Sciences Research Council (EPSRC) under grant EP/M017354/1. The authors are grateful to all project partners for their support, particularly Devon County Council, for providing useful prototype data. Data supporting the presented work can be accessed via the University of Exeter's repository ORE (https://doi.org/10.24378/exe.310). For further information please refer to the project blog at http://blogs.exeter.ac.uk/ramb/.

Notation

The following symbols are used in this paper:

B = width of approach flow;
D_e = equivalent width of a pier without debris;
D_0 = pier width;
d_s = maximum measured scour depth;
$d_{s,EST}$ = maximum estimated scour depth using an empirical equation;
$d_{s,0}$ = maximum scour depth corresponding to baseline (no-debris) scenario;
d_{50} = median particle size of sand;
F = Froude number [$= U/(gh)^{1/2}$];
g = acceleration due to gravity;
h = depth of approach flow;
h_a = height of flow above debris;
h_d = distance of bottom of debris to initial bed;
k_s = sand granular roughness ($2d_{50}$);
$L_{d,x}$ = streamwise (longitudinal) length of debris;
$L_{d,y}$ = spanwise (cross-stream, transversal) length of debris;
Q = flow discharge;
R = flow Reynolds number ($=Uh/\nu$);
R_* = roughness Reynolds number ($= u_* k_s/\nu$);
T_d = thickness of debris;
U = mean velocity of approach flow;
U_{cr} = critical flow velocity for initiation of sediment movement;
u_* = shear velocity;
V_s = volume of scour around the pier at one side of the flume;
x = streamwise coordinate;
y = spanwise coordinate;
z = vertical distance from initial bed;
η_* = relative flow intensity; and
ν = fluid kinematic viscosity.

References

Apsilidis, N., P. Diplas, C. L. Dancey, and P. Bouratsis. 2015. "Time-resolved flow dynamics and Reynolds number effects at a wall-cylinder junction." *J. Fluid Mech.* 776: 475–511. https://doi.org/10.1017/jfm.2015.341.

Arneson, L. A., L. W. Zevenbergen, P. F. Lagasse, and P. E. Clopper. 2012. *Evaluating scour at bridges*. 5th ed. Washington, DC: US Dept. of Transportation.

Beechie, T. J., and T. H. Sibley. 1997. "Relationships between channel characteristics, woody debris, and fish habitat in Northwestern Washington streams." *Trans. Am. Fish. Soc.* 126 (2): 217–229. https://doi.org/10.1577/1548-8659(1997)126<0217:RBCCWD>2.3.CO;2.

Benn, J. 2013. "Railway bridge failure during flooding in the UK and Ireland." *Proc. Inst. Civ. Eng. Forensic Eng.* 166 (4): 163–170. https://doi.org/10.1680/feng.2013.166.4.163.

Bouratsis, P., P. Diplas, C. L. Dancey, and N. Apsilidis. 2017. "Quantitative spatio-temporal characterization of scour at the base of a cylinder." *Water* 9 (3): 227. https://doi.org/10.3390/w9030227.

Bradley, J., D. Richards, and C. Bahner. 2005. *Debris control structures: Evaluation and countermeasures*. Rep. No. FHWA-IF-04-016. Washington, DC: FHWA.

Breusers, H. N. C., G. Nicollet, and H. W. Shen. 1977. "Local scour around cylindrical piers." *J. Hydraul. Res.* 15 (3): 211–252. https://doi.org/10.1080/00221687709499645.

Chang, F. F. M. 1973. *A statistical summary of the cause and cost of bridge failures*. Rep. No. FHWA-RD-75-87. Final Rep. No. 1973. Washington, DC: Federal Highway Administration.

Chang, F. F. M., and H. W. Shen. 1979. *Debris problems in the river environment*. Rep. No. FHWA-RD-79-62. Washington, DC: Federal Highway Administration.

Chanson, H. 2004. *The hydraulics of open channel flow: Basic principles, sediment motion, hydraulic modelling, design of hydraulic structures*. Amsterdam, Netherlands: Elsevier.

Chen, Q., M. Qi, Q. Zhong, and D. Li. 2017. "Experimental study on the multimodal dynamics of the turbulent horseshoe vortex system around a circular cylinder." *Phys. Fluids* 29 (1): 015106. https://doi.org/10.1063/1.4974523.

Chiew, Y. M. 1992. "Scour protection at bridge piers." *J. Hydraul. Eng.* 118 (9): 1260–1269. https://doi.org/10.1061/(ASCE)0733-9429(1992)118:9(1260).

Comiti, F., A. Andreoli, M. A. Lenzi, and L. Mao. 2006. "Spatial density and characteristics of woody debris in five mountain rivers of the Dolomites (Italian Alps)." *Geomorphology* 78 (1): 44–63. https://doi.org/10.1016/j.geomorph.2006.01.021.

Dey, S. 1995. "Three-dimensional vortex flow field around a circular cylinder in a quasi-equilibrium scour hole." *Sadhana* 20 (6): 871–885. https://doi.org/10.1007/BF02745871.

Dey, S., S. K. Bose, and G. L. Sastry. 1995. "Clear water scour at circular piers: A model." *J. Hydraul. Eng.* 121 (12): 869–876. https://doi.org/10.1061/(ASCE)0733-9429(1995)121:12(869).

Diab, R., O. Link, and U. Zanke. 2010. "Geometry of developing and equilibrium scour holes at bridge piers in gravel." *Can. J. Civ. Eng.* 37 (4): 544–552. https://doi.org/10.1139/L09-176.

Diehl, T. 1997. *Potential drift accumulation at bridges*. Washington, DC: US Dept. of Transportation.

Escauriaza, C., and F. Sotiropoulos. 2011. "Lagrangian model of bed-load transport in turbulent junction flows." *J. Fluid Mech.* 666: 36–76. https://doi.org/10.1017/S0022112010004192.

Ettema, R., G. Constantinescu, and B. W. Melville. 2017. "Flow-Field complexity and design estimation of pier-scour depth: Sixty years since Laursen and Toch." *J. Hydraul. Eng.* 143 (9): 03117006. https://doi.org/10.1061/(ASCE)HY.1943-7900.0001330.

Ettema, R., B. W. Melville, and B. Barkdoll. 1998. "Scale effect in pier-scour experiments." *J. Hydraul. Eng.* 124 (6): 639–642. https://doi.org/10.1061/(ASCE)0733-9429(1998)124:6(639).

Ettema, R., T. Nakato, and M. Muste. 2010. *Estimation of scour depth at bridge abutments*. National Cooperative Highway Research Program NCHRP 24-20. Iowa City, IA: Univ. of Iowa.

Frostick, L. E., S. J. McLelland, and T. G. Mercer. 2011. "Users guide to physical modelling and experimentation: Experience of the HYDRALAB network." In *IAHR design manual*. Boca Raton, FL: CRC Press.

Hamill, L. 1998. *Bridge hydraulics*. Boca Raton, FL: CRC Press.

Highways Agency. 2012. "The assessment of scour and other hydraulic actions at highway structures." Vol. 3 of *Design manual for roads and bridges*. Guildford, UK: Highways Agency.

Hjulstrom, F. 1939. "Transportation of detritus by moving water. Part 1: Transportation." In *SP10: Recent marine sediments*, edited by P. D. Trask, 5–31. Tulsa, OK: American Association of Petroleum Geologists.

HR Wallingford, and T. P. O'Sullivan & Partners. 1991. *Hydraulics of highway structures, Part 1*. Rep. No. EX2404. Wokingham, UK: Transport and Road Research Laboratory.

Hunt, B. E. 2009. *Monitoring scour critical bridges*. Washington, DC: Transportation Research Board.

Kail, J. 2003. "Influence of large woody debris on the morphology of six central European streams." *Geomorphology* 51 (1): 207–223. https://doi.org/10.1016/S0169-555X(02)00337-9.

Kamphuis, J. W. 1974. "Determination of sand roughness for fixed beds." *J. Hydraul. Res.* 12 (2): 193–203. https://doi.org/10.1080/00221687409499737.

Khosronejad, A., S. Kang, and F. Sotiropoulos. 2012. "Experimental and computational investigation of local scour around bridge piers." *Adv. Water Resour.* 37: 73–85. https://doi.org/10.1016/j.advwatres.2011.09.013.

Kirkil, G., S. G. Constantinescu, and R. Ettema. 2008. "Coherent structures in the flow field around a circular cylinder with scour hole." *J. Hydraul. Eng.* 134 (5): 572–587. https://doi.org/10.1061/(ASCE)0733-9429(2008)134:5(572).

Lagasse, P. F., P. E. Clopper, L. W. Zevenbergen, W. J. Spitz, and L. G. Girard. 2010. *Effects of debris on bridge pier scour*. Washington, DC: Transportation Research Board.

Laursen, E. M., and A. Toch. 1956. *Scour around bridge piers and abutments*. Ames, IA: Iowa Highway Research Board.

Link, O., C. González, M. Maldonado, and C. Escauriaza. 2012. "Coherent structure dynamics and sediment particle motion around a cylindrical pier in developing scour holes." *Acta Geophys.* 60 (6): 1689–1719. https://doi.org/10.2478/s11600-012-0068-y.

Link, O., F. Pfleger, and U. Zanke. 2008. "Characteristics of developing scour-holes at a sand-embedded cylinder." *Int. J. Sediment Res.* 23 (3): 258–266. https://doi.org/10.1016/S1001-6279(08)60023-2.

Lyn, D., T. Cooper, Y. K. Yi, R. Sinha, and A. R. Rao. 2003. *Debris accumulation at bridge crossings: Laboratory and field studies*. West Lafayette, IN: Purdue Univ.

Magilligan, F. J., K. H. Nislow, G. B. Fisher, J. Wright, G. Mackey, and M. Laser. 2008. "The geomorphic function and characteristics of large woody debris in low gradient rivers, coastal Maine, USA." *Geomorphology* 97 (3–4): 467–482. https://doi.org/10.1016/j.geomorph.2007.08.016.

May, R. W. P., J. C. Ackers, and A. M. Kirby. 2002. *Manual on scour at bridges and other hydraulic structures (CIRIA C551)*. London: CIRIA.

McKibbins, L. D., C. Melbourne, N. Sawar, and C. S. Gaillard. 2006. *Masonry arch bridges: Condition appraisal and remedial treatment (CIRIA C656)*. London: CIRIA.

Melville, B. W. 1975. "Local scour at bridge sites." Ph.D. thesis, School of Engineering, Univ. of Auckland.

Melville, B. W. 1997. "Pier and abutment scour: Integrated approach." *J. Hydraul. Eng.* 123 (2): 125–136. https://doi.org/10.1061/(ASCE)0733-9429(1997)123:2(125).

Melville, B. W., and Y. M. Chiew. 1999. "Time scale for local scour at bridge piers." *J. Hydraul. Eng.* 125 (1): 59–65. https://doi.org/10.1061/(ASCE)0733-9429(1999)125:1(59).

Melville, B. W., and S. E. Coleman. 2000. *Bridge scour*. Littleton, CO: Water Resources Publication.

Melville, B. W., and D. M. Dongol. 1992. "Bridge pier scour with debris accumulation." *J. Hydraul. Eng.* 118 (9): 1306–1310. https://doi.org/10.1061/(ASCE)0733-9429(1992)118:9(1306).

Melville, B. W., and A. J. Sutherland. 1988. "Design method for local scour at bridge piers." *J. Hydraul. Eng.* 114 (10): 1210–1226. https://doi.org/10.1061/(ASCE)0733-9429(1988)114:10(1210).

Müller, G., R. Mach, and K. Kauppert. 2001. "Mapping of bridge pier scour with projection moiré." *J. Hydraul. Res.* 39 (5): 531–537. https://doi.org/10.1080/00221686.2001.9628277.

Oliveira, D. V., P. B. Lourenço, and C. Lemos. 2010. "Geometric issues and ultimate load capacity of masonry arch bridges from the northwest Iberian Peninsula." *Eng. Struct.* 32 (12): 3955–3965. https://doi.org/10.1016/j.engstruct.2010.09.006.

Oliveto, G., and W. H. Hager. 2002. "Temporal evolution of clear-water pier and abutment scour." *J. Hydraul. Eng.* 128 (9): 811–820. https://doi.org/10.1061/(ASCE)0733-9429(2002)128:9(811).

Pagliara, S., and I. Carnacina. 2010. "Temporal scour evolution at bridge piers: Effect of wood debris roughness and porosity." *J. Hydraul. Res.* 48 (1): 3–13. https://doi.org/10.1080/00221680903568592.

Pagliara, S., and I. Carnacina. 2011a. "Influence of large woody debris on sediment scour at bridge piers." *Int. J. Sediment Res.* 26 (2): 121–136. https://doi.org/10.1016/S1001-6279(11)60081-4.

Pagliara, S., and I. Carnacina. 2011b. "Influence of wood debris accumulation on bridge pier scour." *J. Hydraul. Eng.* 137 (2): 254–261. https://doi.org/10.1061/(ASCE)HY.1943-7900.0000289.

Pagliara, S., and I. Carnacina. 2013. "Bridge pier flow field in the presence of debris accumulation." *Proc. Inst. Civ. Eng. Water Manage.* 166 (4): 187–198. https://doi.org/10.1680/wama.11.00060.

Panici, D., and G. A. M. de Almeida. 2017. "Understanding the formation of woody debris jams at bridge piers." In *Proc., 37th IAHR World Congress*. Tokyo: International Association for Hydro-Environment Engineering and Research.

Parola, A. C. 2000. *Debris forces on highway bridges*. Washington, DC: Transportation Research Board.

Parola, A. C., D. J. Hagerty, D. S. Mueller, B. W. Melville, G. Parker, and J. S. Usher. 1997. "The need for research on scour at bridge crossings." In *Proc., Stream Stability and Scour at Highway Bridges: Compendium of Stream Stability and Scour Papers Presented at Conferences*, 1020. Reston, VA: ASCE.

RAIB (Rail Accident Investigation Branch). 2010. *Failure of bridge RDG1 48 (River Crane) between Whitton and Feltham 14 November 2009*. Derby, UK: Dept. for Transport.

Raudkivi, A. J., and R. Ettema. 1983. "Clear-water scour at cylindrical piers." *J. Hydraul. Eng.* 109 (3): 338–350. https://doi.org/10.1061/(ASCE)0733-9429(1983)109:3(338).

Richardson, E. V., and S. R. Davies. 2001. *Evaluating scour at bridges*. 4th ed. Springfield, VA: Federal Highway Administration Report.

Richardson, E. V., L. J. Harrison, J. R. Richardson, and S. R. Davis. 1993. *Evaluating scour at bridges*. 2nd ed. Washington, DC: Federal Highway Administration Report.

Robinson, J. 2000. "Analysis and assessment of masonry arch bridges." Ph.D. thesis, School of Engineering, Univ. of Edinburgh.

Sarhosis, V., S. D. Santis, and G. de Felice. 2016. "A review of experimental investigations and assessment methods for masonry arch bridges." *Struct. Infrastruct. Eng.* 12 (11): 1439–1464. https://doi.org/10.1080/15732479.2015.1136655.

Shen, H. W., V. R. Schneider, and S. S. Karaki. 1966. *Mechanics of local scour*. CER 66 HWS-VRS-SK22. Fort Collins, CO: Colorado State Univ.

Sheppard, D. M., B. W. Melville, and H. Demir. 2014. "Evaluation of existing equations for local scour at bridge piers." *J. Hydraul. Eng.* 140 (1): 14–23. https://doi.org/10.1061/(ASCE)HY.1943-7900.0000800.

Solaimani, N., A. Amini, H. Banejad, and P. Taherei Ghazvinei. 2017. "The effect of pile spacing and arrangement on bed formation and scour hole dimensions in pile groups." *Int. J. River Basin Manage.* 15 (2): 219–225. https://doi.org/10.1080/15715124.2016.1274321.

Toth, E. 2015. "Asymmetric error functions for reducing the underestimation of local scour around bridge piers: Application to neural networks models." *J. Hydraul. Eng.* 141 (7): 04015011. https://doi.org/10.1061/(ASCE)HY.1943-7900.0000981.

Umbrell, E. R., G. K. Young, S. M. Stein, and J. S. Jones. 1998. "Clear-water contraction scour under bridges in pressure flow." *J. Hydraul. Eng.* 124 (2): 236–240. https://doi.org/10.1061/(ASCE)0733-9429(1998)124:2(236).

Unsworth, J. F. 2016. *Design of modern steel railway bridges*. Boca Raton, FL: CRC Press.

van Rijn, L. C. 1993. *Principles of sediment transport in rivers, estuaries and coastal seas*. Amsterdam, Netherlands: Aqua Publications.

Vijayasree, B. A., T. I. Eldho, B. S. Mazumder, and N. Ahmad. 2017. "Influence of bridge pier shape on flow field and scour geometry." *Int. J. River Basin Manage.* 1–21 https://doi.org/10.1080/15715124.2017.1394315.

Wallerstein, N., S. Arthur, and D. Sisinngghi. 2010. "Towards predicting flood risk associated with debris at structures." In *Proc., IAHR APD Conf. 2010*. Tokyo: International Association for Hydro-Environment Engineering and Research.

Wellwood, N., and J. Fenwick. 1990. "A flood loading methodology for bridges." In *Proc., Australian Road Research Board (ARRB) 15th Conf.*. Melbourne, VIC, Australia: Australian Road Research Board.

Yalin, M. S. 1972. *Mechanics of sediment transport*. New York: Pergamon Press.

Yalin, M. S., and A. M. F. da Silva. 2001. *Fluvial processes*. Delft, Netherlands: International Association for Hydro-Environment Engineering and Research.